# Enhanced RFI Detection in Imbalanced Astronomical Observations Using Weakly Supervised GANs

Arush S. Sharma and Marwan Krunz

Department of Electrical and Computer Engineering, University of Arizona, Tucson, USA

{arushsharma, krunz}@arizona.edu

Abstract—Radio astronomical observations are plagued by radio frequency interference (RFI) caused by a variety of man-made signals, e.g., cellular, automotive radar, satellite, GPS, etc. Both the wireless and radioastronomy communities have great interest in identifying RFI in the vicinity of the telescopes in real-time. This paper proposes the use of Generative Adversarial Networks (GANs) in the context of weakly supervised learning as a means to enhance the machine learning (ML) based detection of RFI in captured astronomical scans. Weakly supervised training is particularly appropriate when only a small subset of captured data is labeled, as is the case with many radioastronomical datasets. Such "class imbalance" in the training dataset hampers the classifier's performance, particularly in terms of identifying the minority class samples with RFI, which is often the class of greater interest. Applying weakly or semi-supervised training to GANs addresses the class imbalance challenges. Our study is based on scans obtained from the 12-meter Alma-like Observatory at Kitt Peak, Arizona. We rely on the experience of radio astronomers to manually label the channels in a small fraction of the captured scans as "clean" or "dirty". The remaining channels of 4 GHz of the observed spectrum (95% of the scans) are unlabeled. We first use our human-labeled data as ground truth and train a baseline classifier in a supervised manner. Subsequently, we explore two approaches for weakly supervised learning. The first approach uses a combination of an autoencoder and conditional GAN, while the second approach uses a semi-supervised GAN (SGAN). Both techniques harness the features learned from the unlabeled dataset to train the generator and discriminator of a GAN. In the first approach, the trained generator is used to synthesize the dirty data, while in the second approach, the trained discriminator is modified to act as a clean/dirty RFI classifier. Simulations under extremely imbalanced training samples show that the SGAN approach can significantly improve the F1-score and True Positive Rate (TPR) relative to the baseline classifier.

Index Terms—RF Interference, radioastronomy, CNN, GANs, Machine Learning, Autoencoder

#### I. INTRODUCTION

Radioastronomy (RA) telescopes provide vital scientific observations related to Earth's environment, solar system, cosmos, galaxies, formation of pulsars and stars, etc. They operate over a wide range of Fourier bandwidth ranging from 2 MHz to 1000 GHz, and above. The ITU-R RA.314-10 [1] presents a compilation of frequency bands used for RA observations, primarily encompassing chemicals and molecules.

Radio Frequency Interference (RFI) occurs when unwanted terrestrial or satellite transmissions lead to undesired emissions within RA bands. Harmful RFI not only makes RA observations inaccurate or even false during the post-processing analysis but also often triggers repeating the measurement, at a high cost in terms of telescope time and manpower. Figure 1 shows one such instance of RFI in a scan gathered from the 12-meter Alma-like telescope at Kitt Peak Arizona. The antenna temperature is a measure of the power received by the telescopic antenna from an astronomical source. The frequency offset represents a variance from the central observation frequency, set at 88 GHz for this particular instance.

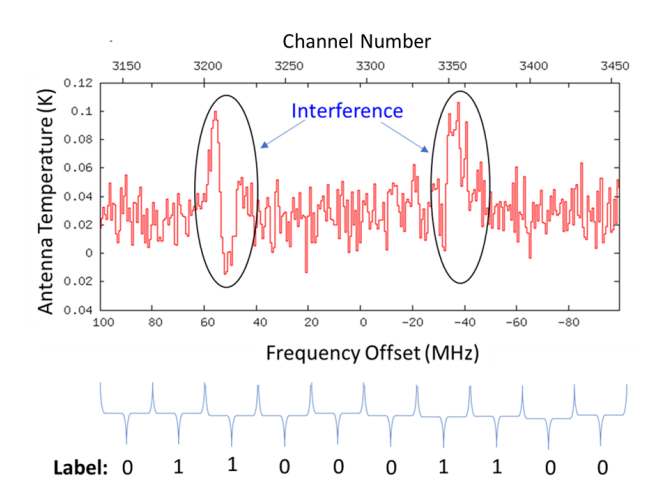


Fig. 1. RFI in a typical scan. Ten 20 MHz channels in the observed band are labeled as '0'(clean) or '1'(dirty).

Radio telescopes are built to detect extremely faint emissions, which arrive at lower power levels than man-made signals, necessitating greater sensitivity than standard wireless receivers. Consequently, telescopes are situated in remote areas far from urban centers. Advances in radio astronomy [2] have significantly increased sensitivity to faint cosmic signals. Therefore, minimizing the impact of RFI is crucial.

An essential step in this direction is real-time RFI identification. Currently, operators or engineers visually inspect gathered astronomical data for RFI, a time-consuming process. Machine learning (ML) techniques offer a solution

for inspection and real-time detection. However, in radio astronomy, challenges arise due to two main factors. First, much of the collected data lacks RFI labels. Second, there's a class imbalance issue, where the number of clean samples far exceeds that of dirty ones. This imbalance biases ML classifiers toward the majority class, hindering effective learning of minority class features, which are often of greater interest.

Conventional methods for addressing class imbalance include undersampling and oversampling. Undersampling randomly removes majority class samples to create a balanced but smaller training set, while oversampling duplicates minority class samples to reduce the imbalance. However, oversampling doesn't increase feature variety. Techniques like SMOTE [3] generate synthetic minority class data considering only its neighborhood, ignoring the majority class distribution. This can lead to noisy synthetic samples near majority class ones, blurring the decision boundary between the classes.

In this paper, we leverage the richness of Generative Adversarial Networks (GANs) to enable weakly supervised learning from unlabelled data. Two GAN-related approaches are studied. In both approaches, the generator plays a pivotal role in enhancing the classifier's performance under data scarcity by generating synthetic samples that augment the training set, thereby mitigating the challenges posed by limited training data and overcoming the class imbalance. The main contributions of the paper are as follows:

- Based on our previous work [4], we consider two ML-based binary RFI classifiers: a Convolutional Neural Network Bidirectional Long Short Term Memory (CNN-BiLSTM) and a Deep CNN, and study their performance by varying the imbalance ratio of the labeled training dataset. We observe that with an increase in the imbalance ratio, the performance of both classifiers degrades in terms of classification accuracy and True Positive Rate (TPR).
- To address the class imbalance problem, we first introduce a weakly supervised learning approach that uses the combination of an autoencoder and a conditional GAN (cGAN) to generate synthetic dirty samples and compensate for the imbalanced scenario in the training set. The original (baseline) classifier is then trained on the augmented training samples. We then introduce a second approach that relies on a semisupervised GAN (SGAN), wherein a classifier is stacked on the discriminator to leverage the features of unlabeled data. Performance evaluation of the two approaches demonstrates comparable performance.
- We continue our performance evaluation with the SGAN approach. The test accuracy and F-1 score are found to be 94.75% and 0.857, respectively. Furthermore, we test the robustness of SGAN by considering different proportions of the labeled ground truth data along with different imbalance ratios of. We find that even under severely imbalanced training samples, the SGAN ap-

proach has a relatively higher TPR in terms of accurately detecting RFI.

#### II. RELATED WORK

Various prior studies have introduced approaches for detecting RFI utilizing signal processing or machine learning techniques. Ford et al. [5] provided a summary of various RFI mitigation techniques in radio astronomy. One such technique operates in the time domain and uses a threshold-based using Mean Absolute Deviation (MAD) estimator. A second technique excises RFI either in temporal or spectral domains using spectral kurtosis which can indicate the presence of gaussian or nongaussian components in the signal. In a third technique, spatial excision with adaptive beamforming is used to minimize RFI effects by creating a null in the beam pattern along the direction of interference. Cancellation is yet another technique that requires subtracting the RFI from the received astronomical signal. RFI is first detected and estimated using separate sensors before it is subtracted from RFI-corrupted data.

Mosiane et al. [6] investigated ML algorithms for RFI detection in Karoo Radio Telescope (KAT-7) data, using semi-automated AO Flagger software to flag the data. They employed three ML algorithms (K-Nearest Neighbor, Random Forest, and Naive Bayesian) for classification and compared their performance.

Maan et al. [7] highlighted Fourier-domain excision's effectiveness in improving the detection of faint cosmic signals by enhancing the signal-to-noise ratio. They introduced novel Fourier-domain filtering techniques that efficiently remove periodic RFI while preserving the spectral characteristics of astronomical signals. By identifying RFI periodicity in the Fourier domain, these methods selectively remove corresponding frequency components. Testing on GMRT data validated successful periodic RFI removal while preserving astronomical signals.

Akeret et al. [8] proposed RFI mitigation using CNNs, employing U-Net architecture to classify clean signals and RFI in time-domain radio telescope data. Initially developed for biomedical image segmentation [9], U-Net extends conventional CNNs. Simulated data with perfect ground truth was generated using the HIDE & SEEK package. The U-Net model achieved an AUROC of 0.959 on this dataset. Real astronomical data from Bleien Observatory, processed with the SUMTHRESHOLD flagger, had imperfect ground truth due to incorrect flagging. Despite this, training the U-Net model on the dataset yielded an AUROC of 0.88.

Chakraborty et. al. [10] proposed collaborating with cellular networks in RFI cancellation. Their approach uses signal characterization and eigenspaces to adaptively cancel the interference, leading to improved data quality and increased throughput for radio astronomy observations. Along with real-world astronomical data, simulated LTE signals (downlink and uplink) were used as RFI. The authors showed

that with such collaboration, it is possible to remove 89.04% of the RFI coming from cellular sources.

Sobjerg et al. [11] proposed using spectral kurtosis for RFI detection. They found that while normal kurtosis is effective for pulsed sinusoidal signals with short duty cycles, it lacks sensitivity for long-duty cycles and continuous signals. Spectral kurtosis, however, excels in detecting duty cycles above 15%, albeit with reduced sensitivity to short duty cycles. The authors suggested combining both methods for improved RFI detection.

Vos et al. [12] presented a RFI mitigation approach that aims to separate RFI-corrupted spectrogram observations into two components that are signal of interest and RFI. The authors used the simulated data and RFI signals from HIDE & SEEK package and applied GAN framework to achieve their objective.

#### III. ASTRONOMICAL DATASET

# A. ARO Telescope at Kitt Peak



Fig. 2. 12-meter dish telescope at Kitt Peak, Tucson. Source: NOIRLAB, 2024. https://noirlab.edu/public/images/noirlab-05290/

The Arizona Radioastronomy Observatory (ARO) manages a range of telescopes, which includes a 12-meter Almalike telescope situated at Kitt Peak and a Submillimeter telescope located at Mt. Graham. The 12-meter telescope has operating frequencies that range from 68 GHz to 180 GHz [13] supporting both spectral lines and continuum observations. Among various observing modes of the telescope, astronomical observations for our analysis were gathered using position-switched mode. In this mode, the telescope alternates between ON and OFF positions according to a given azimuthal offset. The OFF position is devoid of any emissions. During the ON position, the telescope is directed towards the astronomical source, capturing and recording the emitted temperature from this source. The same logic holds true when the telescope is pointing towards OFF position. The difference in the temperatures between ON and OFF is normalized, i.e., (ON-OFF)/OFF, signifying the source's antenna temperature or brightness temperature. The positionswitched mode follows an OFF-ON-ON-OFF pattern, with 30-second durations for both ON and OFF periods. Each sequence of ON-OFF is termed a repeat. In a standard scan, the antenna temperature is averaged over six of these repeats. Figure 2 shows the telescope with a 12-meter diameter dish at Kitt Peak, Tucson.

## B. Measurement Setup

The astronomical scans obtained from the ARO telescope are in Single Dish Data (SDD) format, which can be processed using a proprietary Linuxpops CLASS package on a Unix machine. The dataset comprises 515 scans encompassing diverse sky frequencies within the ranges of 78-82 GHz, 86-90 GHz, and 102.7-106.7 GHz. Each scan is 4000 MHz wide. These scans yield temperature measurements normalized to Kelvin for a specific sky area, determined by the telescope's orientation at particular azimuth and elevation angles. Observations for a specific sky frequency include both vertical and horizontal polarization. The default duration for a scan is six minutes. In our scans, interference becomes apparent when the azimuth angle exceeds 200 degrees. In our previous study, [4], from a qualitative perspective, we could confidently identify the RFI over a small portion of the spectrum (±100 MHz) from the center sky frequency of the observation. The distortion effects in the brightness temperature of an astronomical source due to RFI are visible in the scans.

Figure 1 shows an example of an interference that a human could eyeball. We divide the scans into nonoverlapping channels of 20 MHz wide as these channels could capture such interference effects. Each such channel is assigned a binary label, where 0 signifies an RFI-free channel and 1 signifies a channel with unacceptable RFI. The remaining portion of the scan consisting of 190 channels for which the qualitative interpretation seems to be difficult is left unlabeled. The frequency resolution for each scan is 0.625 MHz, which implies that a 20 MHz wide channel contains 32 temperature values. These channels are used as an input to the ML classifiers. In our dataset, 4,673 channels are labeled and 98,327 channels are unlabeled. Given the labeled channels, the total number of samples in the "clean" and "dirty" classes are 3,898 and 775 respectively. The dataset is split into 80/20 for training and testing.

## IV. PERFORMANCE WITH VARYING IMBALANCE RATIO

As shown in Figure 3, we study the performance of two classifiers which are CNN-BiLSTM and Deep CNN by varying the imbalance ratio on the labeled dataset where TNR is True Negative Rate and CA is Classification Accuracy. The default imbalance ratio in our dataset is 5 and this ratio is increased by randomly undersampling the "dirty" class samples. It can be observed that with an increase in the imbalance ratio, the classifier(s) indeed perform well in detecting "clean" class samples but lose out on the information related to "dirty" class samples. This hurts their RFI detection capability which is indicated by the reduction in their TPR.

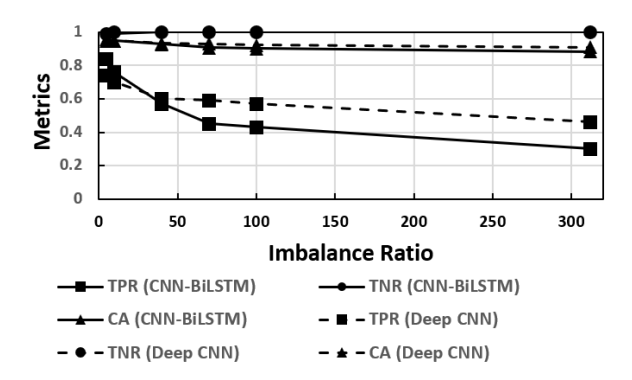


Fig. 3. Impact on classifiers with varying imbalance ratio.

# V. BALANCING DATASET USING GENERATIVE TECHNIQUES

#### A. Basics of GAN

GAN was proposed in 2014 by Goodfellow et al. [14]. As the name suggests, GAN generates new data by learning the distribution of data in an adversarial way. GAN is composed of two networks which are "generator" and "discriminator". The input to the generator is latent space which is typically a random noise vector. The generator creates synthetic data whereas the latter predicts whether the input data that it receives from the generator is real or synthetic/fake. During the adversarial training, the generator always tries to outsmart the discriminator according to the 2-player min-max game. After the GAN training, ideally both the networks converge to a Nash equilibrium where the discriminator has a 50% chance of making a mistake.

Suppose that  $x_r \sim p_{data}$  is a sample belonging to real data distribution,  $x_g \sim p_g$  is a generated sample from the generator G by mapping the noise vector  $z \sim p_z$ , whose distribution is close to that of  $p_{data}$ . The discriminator D takes in a sample (either  $x_r$  or  $x_g$ ) and outputs the probability of the sample being real. The objective function of GAN can be formalized as follows:

# B. Autoencoder+conditional GAN Approach

Fig. 4. Structure of the Autoencoder.

Existing works [15] in the literature have made use of using a combination of autoencoders with GANs. We couple the autoencoder with GAN and leverage the features learned

from the unlabeled data. Figure 4 shows the architecture of the autoencoder considered for our analysis. At first, the autoencoder is trained with unlabeled samples. At this moment, the autoencoder doesn't have any explicit class knowledge but it learns the overall feature representation. Subsequently, the knowledge of the autoencoder is transferred to GAN modules by initializing the weights of GAN with that of the autoencoder. To make this happen, the generator has to match the topology of the decoding section of the autoencoder. Similarly, the discriminator matches with the encoding section of the autoencoder except for the output layer which is a single node with a sigmoid activation. The initialized weights of the GAN are then refined by training the GAN with the labeled data.

The training of GAN is performed conditionally in a balanced way. The input to the generator is a random noise vector N(0,1) with size 100 and the latent vector which is typically a class label in one hot encoded format. The input to the discriminator is the input data (either real or fake) along with the latent vector. The latent vector helps drive the generator towards producing synthetic samples of a particular class. After the training of conditional GAN is completed, we generate synthetic "dirty" samples and augment them to the labeled ground truth such that the classes are balanced. Finally, the classifier with the same architecture as that of the discriminator or encoder part of the autoencoder is trained on the augmented training set. A total of 200 epochs are considered in our simulations. We use Adam as an optimizer with a learning rate of  $2 \times 10^{-4}$ .

# C. Semi-supervised GAN Approach

SGAN has been used by many researchers in vari-

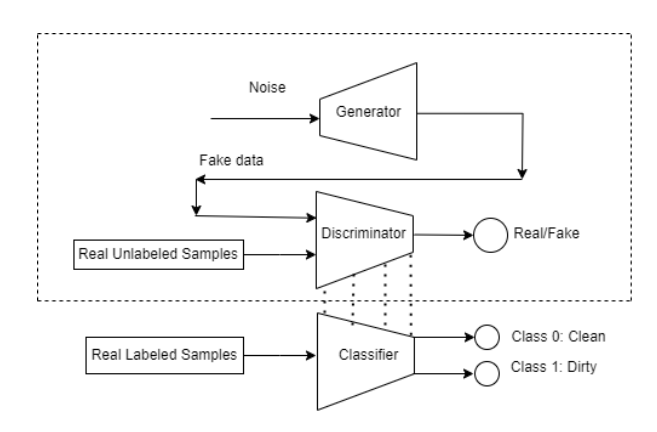


Fig. 5. Semisupervised GAN pipeline.

ous areas wherein the input data is typically 2-dimensional representing an image [16]–[18]. It is an extension of a GAN wherein three models (Generator, Discriminator, and Classifier) are trained concurrently making use of labeled and unlabelled data. As can be seen in Figure 5, the discriminator is fed with "real unlabeled" samples and synthetic samples from the generator and predicts whether it is real or fake during the training.

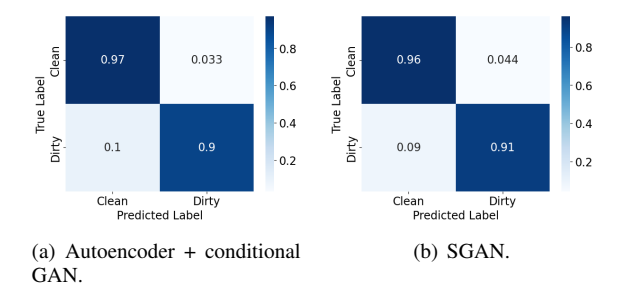


Fig. 6. Confusion matrices for the Autoencoder + conditional GAN and SGAN approaches.

Except for the output layer, the discriminator shares the remaining layers with the classifier. The classifier is fed with "real labeled" samples with an equal number of samples from the "clean" and "dirty" classes and is trained in a supervised way. The idea behind the SGAN approach is that as the discriminator becomes better at learning the features from the large unlabeled dataset, it benefits the classifier as the classifier uses the discriminator from the transfer learning point of view.

#### VI. PERFORMANCE EVALUATION

We compare the performance of the Autoencoder + conditional GAN and SGAN approaches as can be seen from the confusion matrices shown in Figures 6(a) and 6(b). It can be observed that both techniques perform well as they utilize the features learned from the unlabeled dataset. SGAN marginally performs well in terms of TPR.

We continue to evaluate the performance of SGAN. Fig-7(a) and 7(b) show the architecture for the discriminator and classifier respectively. Except for the output layer they both have the same architecture. As our data is 1-dimensional, we use three 1D CNN layers as it can capture salient features from the input through the kernel and pooling. The layer before the output layer is flattened and is passed through the dense layer. All layers prior to output use the LeakyReLU activation function and a dropout of 0.4 has been added as a regularizer. In the discriminator, the output layer has a sigmoid activation function to distinguish between real and fake whereas in the classifier, the output layer uses softmax activation. The input to the discriminator and classifier is normalized between -1 and +1. The generator shown in Figure 7(c) takes in random noise N(0,1) vector of size 100 and the output layer uses the tanh activation function.

A total of 200 epochs are considered during training. Adam is used as an optimizer with a learning rate of  $2 \times 10^{-4}$ .

Figures 8(a) and 8(b) show the confusion matrix of the standalone classifier and SGAN-based classifier respectively. The standalone classifier is trained based on limited labeled data only. The test accuracy of a standalone classifier is 93.37% whereas for the classifier with GAN training is 94.75%. F-1 score is another performance metric suitable for binary classification with imbalanced datasets [19]. F-1

score is the harmonic mean of precision and recall providing a balance between the two. The F-1 score for the standalone classifier is 0.763 and for the SGAN-based classifier is 0.857.

Table I summarizes the performance comparison of the standalone classifier and SGAN-based classifier.

TABLE I COMPARISON OF STANDALONE CLASSIFIER WITH SGAN-BASED CLASSIFIER

Performance Metrics	Standalone classifier	SGAN based classifier
True Positive Rate	0.65	0.95
False Negative Rate	0.35	0.052
True Negative Rate	0.99	0.95
False Positive Rate	0.009	0.053
F-1 Score	0.763	0.857
Test Accuracy	93.37%	94.75%

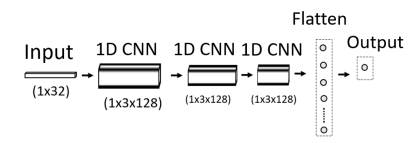
#### A. Robustness of SGAN

We test the robustness of SGAN by considering different proportions of the labeled data selected at random. We consider four different scenarios where 10%, 40%, 70%, and 100% of the labeled data are considered at a time. For each case, the standalone classifier is first trained with the corresponding amount of labeled data. Subsequently, we perform the SGAN training as described in Section V-C where the corresponding amount of labeled data is fed to the classifier. Subsequently, we increase the imbalance ratio to 10 and replicate the experimental setup for further investigation.

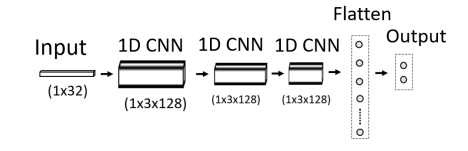
Figure 9 shows the comparison of the F-1 score for the standalone and SGAN-based classifier. It can be observed that the SGAN-based classifier clearly outperforms the standalone classifier in all cases.

#### VII. CONCLUSIONS AND FUTURE WORK

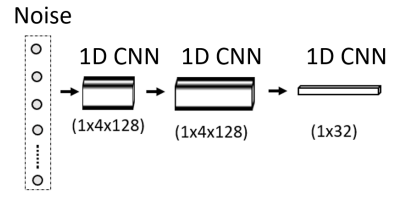
In this work, we enhanced the performance of a classifier in detecting RFI from astronomical data. At first, since our labeled dataset is imbalanced, we showed that with a severe increase in the imbalance ratio, the classifier performs poorly in detecting RFI channels. Since the amount of unlabeled data was far more than that of labeled data, we considered two approaches in the context of weakly supervised learning. First, we used the coupling of autoencoder with conditional GAN and augmented the training dataset with synthetic RFI samples. Subsequently, we used the SGAN technique and compared their performance. Furthermore, we continued to evaluate the SGAN and the results in terms of the TPR clearly show that the SGAN outperforms the standalone classifier. We further analyzed the robustness of SGAN by considering different proportions of the labeled data (10%, 40%, 70%, 100%) along with an imbalance ratio of 5 and 10. We conclude that SGAN's performance outperforms the standalone classifier in all cases. We only considered CNNs in the SGAN framework. In the future, we intend to explore different Deep Neural Network architectures for our SGAN framework. Also, there's room for improvement in reducing



(a) Architecture of a discriminator.

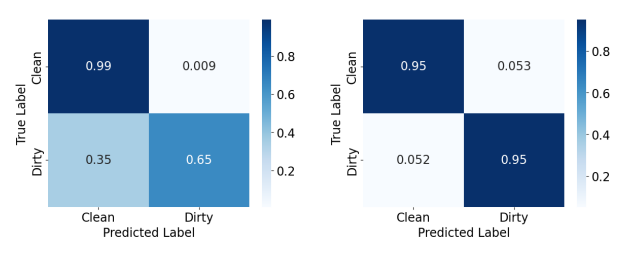


(b) Architecture of a classifier.



(c) Architecture of a generator.

Fig. 7. Architectures of a SGAN.



- (a) Standalone classifier.
- (b) Classifier with SGAN.

Fig. 8. Confusion matrices for the classifier without and with SGAN training.

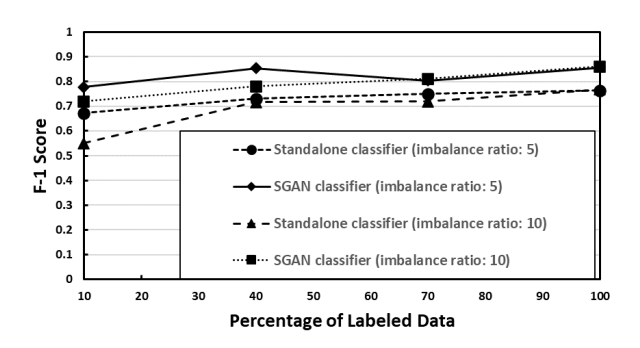


Fig. 9. F-1 score comparison.

the False Positives albeit it's not as serious as False Negatives in our case.

#### ACKNOWLEDGMENT

This research was supported in part by NSF (grants # 2229386 and 1822071) and by the Broadband Wireless Access & Applications Center (BWAC). Any opinions, findings, conclusions, or recommendations expressed in this paper are those of the author(s) and do not necessarily reflect the views of NSF. We like to acknowledge George Reiland and Arizona Radio Observatory for providing us with the astronomical dataset. Additionally, we like to thank Sopan Sarkar for his invaluable insights and comments.

#### REFERENCES

- R. Series, "Preferred frequency bands for radio astronomical measurements," tech. rep., Technical Report 10, International Telecommunication Union (ITU), 2010.
- [2] N. R. Council et al., Spectrum Management For Science in the 21st century. National Academies Press, 2010.

- [3] N. V. Chawla, K. W. Bowyer, L. O. Hall, and W. P. Kegelmeyer, "SMOTE: Synthetic minority over-sampling technique," *Journal of Artificial Intelligence Research*, vol. 16, pp. 321–357, 2002.
- [4] A. S. Sharma, M. Krunz, G. Reiland, and D. P. Marrone, "Identification of RF interference in astronomical observations using weakly supervised machine learning classifiers," in *Proceedings of the Int'l ACM Conference on Modeling Analysis and Simulation of Wireless and Mobile Systems*, pp. 291–295, 2023.
- [5] J. M. Ford and K. D. Buch, "RFI mitigation techniques in radio astronomy," in *Proc. of the IEEE Geoscience and Remote Sensing* Symposium, pp. 231–234, 2014.
- [6] O. Mosiane, N. Oozeer, A. Aniyan, and B. A. Bassett, "Radio frequency interference detection using machine learning," in *Proceedings of the IOP Conference Series: Materials Science and Engineering*, vol. 198, 2017.
- [7] Y. Maan, J. van Leeuwen, and D. Vohl, "Fourier domain excision of periodic radio frequency interference," *Astronomy & Astrophysics*, vol. 650, 2021.
- [8] J. Akeret, C. Chang, A. Lucchi, and A. Refregier, "Radio frequency interference mitigation using deep convolutional neural networks," *Astronomy and Computing*, vol. 18, pp. 35–39, 2017.
- [9] O. Ronneberger, P. Fischer, and T. Brox, "U-net: Convolutional networks for biomedical image segmentation," in *Proceedings of the Medical Image Computing and Computer-Assisted Intervention – MICCAI*, pp. 234–241, Springer, 2015.
- [10] S. Chakraborty, G. Hellbourg, M. Careem, D. Saha, and A. Dutta, "Collaboration with cellular networks for RFI cancellation at radio telescope," *IEEE Transactions on Cognitive Communications and Networking*, 2023.
- [11] S. S. Søbjærg, J. Svoboda, J. E. Balling, and N. Skou, "Detection of radio-frequency interference in microwave radiometers using spectral kurtosis," in *Proceedings of the IEEE International Geoscience and Remote Sensing Symposium*, pp. 7141–7144, 2012.
- [12] E. E. Vos, P. F. Luus, C. J. Finlay, and B. A. Bassett, "A generative machine learning approach to RFI mitigation for radio astronomy," in *Proceedings of the IEEE 29th International Workshop on Machine Learning for Signal Processing (MLSP)*, pp. 1–6, 2019.
- [13] J. Mangum, User's Manual for the NRAO 12 Meter Millimeter-Wave Telescope Kitt Peak, Arizona. NRAO Tucson, AZ, 2000.
- [14] I. Goodfellow, J. Pouget-Abadie, M. Mirza, B. Xu, D. Warde-Farley, S. Ozair, A. Courville, and Y. Bengio, "Generative adversarial nets," *Advances in neural information processing systems*, vol. 27, 2014.
- [15] G. Mariani, F. Scheidegger, R. Istrate, C. Bekas, and C. Malossi, "BAGAN: Data augmentation with balancing GAN," arXiv preprint arXiv:1803.09655, 2018.
- [16] A. Odena, "Semi-supervised learning with generative adversarial networks," arXiv preprint arXiv:1606.01583, 2016.
- [17] Y. Gao, P. Zhai, and K. M. Mosalam, "Balanced semisupervised generative adversarial network for damage assessment from low-data imbalanced-class regime," *Computer-Aided Civil and Infrastructure Engineering*, vol. 36, no. 9, pp. 1094–1113, 2021.
- [18] Y. Yang, F. Nan, P. Yang, Q. Meng, Y. Xie, D. Zhang, and K. Muhammad, "GAN-based semi-supervised learning approach for clinical decision support in health-IoT platform," *IEEE Access*, vol. 7, pp. 8048–8057, 2019.
- [19] N. V. Chawla, N. Japkowicz, and A. Kotcz, "Special issue on learning from imbalanced data sets," ACM SIGKDD Explorations Newsletter, vol. 6, no. 1, pp. 1–6, 2004.